

Impact of the spatial distribution of imperviousness on the hydrologic response of an urbanizing basin

Alfonso I. Mejía¹ and Glenn E. Moglen^{2*}

¹ Department of Civil and Environmental Engineering, University of Maryland, College Park, MD 20742, USA

² Department of Civil and Environmental Engineering, Virginia Tech, Falls Church, VA 22043, USA

Abstract:

An event-based model is used to investigate the impact of the spatial distribution of imperviousness on the hydrologic response of a basin characterized by an urban land use. The impact of the spatial distribution of imperviousness is investigated by accounting for its location within the basin when estimating the generated runoff and the hydrologic response. The event model accounts for infiltration and saturation excess; the excess runoff is routed to the outlet using a geomorphologic unit hydrograph. To represent the spatial distribution of rainfall and imperviousness, radar and remotely derived data are used, respectively. To estimate model parameters and analyse their behaviour, a split sample test and parameter sensitivity analysis are performed. From the analysis of parameters, we found the impervious cover tends to increase the sensitivity and storm dependency of channel routing parameters. The calibrated event model is used to investigate the impact of the imperviousness gradient by estimating and comparing hydrographs at internal locations in the basin. From this comparison, we found the urban land use and the spatial variability of rainfall can produce bigger increases in the peak flows of less impervious areas than the most urbanized ones in the basin. To examine the impacts of the imperviousness pattern, scenarios typifying extreme cases of sprawl type and clustered development are used while accounting for the uncertainty in parameters and the initial condition. These scenarios show that the imperviousness pattern can produce significant changes in the response at the main outlet and at locations internal to the overall watershed. Overall, the results indicate the imperviousness pattern can be an influential factor in shaping the hydrologic response of an urbanizing basin. Copyright © 2010 John Wiley & Sons, Ltd.

KEY WORDS impervious surfaces; urbanization; flooding

Received 28 October 2009; Accepted 12 April 2010

INTRODUCTION

There is growing interest in the hydrology of urbanizing basins (Delleur, 2003; DeFries and Eshleman, 2004). Traditionally, urban hydrology focused on the hydraulic representation of floods on streets and pipes, and the design of water distribution and sewer systems (Delleur, 2003). Later, knowledge about the impacts of urbanization on the environment led to the analysis and modelling of pollutants in urban systems, and to the implementation of design techniques (often collectively referred to as best management practices and, more recently, low impact development) for reducing some of the effects of urban growth on water resources (Delleur, 2003). Currently, along with sustainability concerns and requirements for integrative water resources designs, there are pressing scientific and practical needs to better understand the relationship between local and large-scale land-use changes from urbanization (Vörösmarty *et al.*, 2000; Pielke, 2005). Scientific needs are clear in the context of climate change studies and in land surface modelling, where the effects of urbanization on land processes can be an important control (Pielke, 2005). Practical needs

arise from the increasing relevance of basin-wide planning. A good example of these practical needs are large-scale restoration projects, where the ability to understand present and future urban growth can be as important as predicting climatic, hydrologic, and other natural variability (Claggett *et al.*, 2004). This need has been accentuated by the ubiquitous presence of sub-urban growth or sprawl, which has reduced the land area assumed to be in natural conditions (Vörösmarty *et al.*, 2000).

To meet these needs, and for research and design considerations as well, the application of knowledge about hydrological processes, and analytical methods used routinely in hydrology, is slowly expanding to include the effects of land-use change from urbanization. Some of these applications include, in addition to the well-established stormwater and sewer design models [e.g. SWMM5 (Rossman, 2007) and MIKE URBAN (Mikkelsen *et al.*, 2005)], conceptual rainfall–runoff models for urbanized basins (Burgess *et al.*, 1998), variable source area-based models (Valeo and Moin, 2001; Easton *et al.*, 2007), physically based distributed modelling (Cuo *et al.*, 2008), derived distribution methods (Guo and Adams, 1998), geographic information system (GIS)-based modelling (Moglen and Beighley, 2002) and unit hydrograph and routing-based methods (Rodriguez *et al.*, 2005). Besides investigating and recognizing the applicability of hydrologic concepts and methods to

*Correspondence to: Glenn E. Moglen, Department of Civil and Environmental Engineering, Virginia Tech, Room 424-Northern Virginia Center, Falls Church, VA 22043, USA. E-mail: moglen@vt.edu

urbanizing basins, these applications emphasize the need for analytical and modelling studies at a range of basin scales, and the increasing importance of the urban land-use condition.

Conclusions from the analysis of observations (e.g. streamflows, channel morphology, and water quality) and modelling efforts offer a coherent diagnosis of the impacts of urbanization (Walsh *et al.*, 2005; Miller *et al.*, 2007). The diagnosis typically includes increases in peak flows, decreases in the time for flows to peak, channel widening, and degradation of stream water quality and ecology from pollutants and changing flow regimes (Leopold, 1968; Sauer *et al.*, 1983; Walsh *et al.*, 2005; Moglen and Shivers, 2006; Miller *et al.*, 2007). Despite the common diagnosis of the effects of urbanization on water resources, the investigation of the role played by the imperviousness pattern has received little attention. Mostly qualitative evidence has been reported indicating that the pattern can play an important role (Valeo and Moin, 2001; Poff *et al.*, 2006).

The main objective of this article is to investigate the impact of the imperviousness pattern on the hydrologic response. We use an event-based model to estimate runoff in space (Troch *et al.*, 1994), and the flow hydrograph at the outlet, where the outlet can be any point on the channel network (Olivera and Maidment, 1999; Nicóтина *et al.*, 2008). The event model incorporates the spatial distribution of imperviousness by discretizing the basin into a grid of regular squares and by routing runoff generated on each grid cell to the outlet (Olivera and Maidment, 1999; Nicóтина *et al.*, 2008). Before applying the event model, we perform a model calibration and a parameter sensitivity analysis. Lastly, the calibrated event model is used to compare the hydrograph at various internal locations in the basin and to compare different imperviousness scenarios.

MODELLING APPROACH

This section describes the modelling approach used to partition rainfall into runoff, route the excess rainfall to the outlet, and separate baseflow contributions. The goal with the modelling approach is to account for the spatial distribution of imperviousness and, at the same time, maintain a simple parsimonious model.

Runoff generation

We used for runoff generation an approach similar to the one implemented by Troch *et al.* (1994). However, we start with a more general assumption about the subsurface transmissivity profile (Duan and Miller, 1997). This approach was chosen because it is event based, requires few parameters, accounts for spatially distributed imperviousness data, evidence indicates its applicability to conditions in our selected basin and climate, and because this approach is computationally efficient. The runoff generation approach uses a topographic index to estimate the initial saturated areas and track the amount

of saturation during the storm event, and uses Philip's infiltration equation to simulate infiltration excess (Philip, 1960; Beven and Kirkby, 1979). The method is briefly described here but more complete explanations can be found elsewhere (Troch *et al.*, 1994; Duan and Miller, 1997).

Runoff from saturation excess. We use the following condition to estimate the initial saturated areas in the basin (Duan and Miller, 1997):

$$1 - \frac{\bar{\delta}}{n} \geq \frac{\bar{\xi}}{\xi^{1/n}} \quad (1)$$

where $\bar{\delta}$ is the ratio of the initial average storage deficit, \bar{S} (L), to the maximum storage deficit, S_{\max} (L). \bar{S} is an initial condition of the model in this case and S_{\max} can be interpreted as some effective soil depth. n is the dimensionless generalizing factor for the transmissivity profile, it allows theoretically the consideration of various profile forms (e.g. linear, power, and exponential) (Ambroise *et al.*, 1996; Duan and Miller, 1997). The parameter n also determines the form of the recession curve and affects the distribution of saturated areas and local deficits (Ambroise *et al.*, 1996). ξ is defined as:

$$\xi = \frac{a}{T_0 \tan \beta} \quad (2)$$

where a is the area drained per unit contour width (L), T_0 is the transmissivity constant (L^2/T), and $\tan \beta$ is the local topographic slope. $\bar{\xi}$ is the expected value of ξ . The variables a and $\tan \beta$ can be estimated from the Digital Elevation Model (DEM) and vary locally. S_{\max} and T_0 can be estimated from calibration and they are assumed to be basin-wide constants in this application as done by Franchini *et al.* (1996).

To determine the local deficits at the start of the simulation, the following expression is used (Duan and Miller, 1997):

$$\delta_i = n - \frac{\xi^{1/n}}{\bar{\xi}} (n - \bar{\delta}) \quad (3)$$

The local scaled storage deficit, δ_i , is dimensionless and equal to the ratio of the local deficit (S_i) and S_{\max} . New saturated areas during the storm event are formed where and when δ_i becomes equal to or less than 0. The rate at which δ_i is filled depends on the infiltration capacity or rainfall rate. A similar assumption was previously used by Woods and Sivapalan (1999).

Runoff from infiltration excess. We use Philip's infiltration equation (Philip, 1960), under the assumption of the time compression approximation, to simulate infiltration excess (Milly, 1986). The infiltration equation is as follows (Milly, 1986):

$$f_i^*(F_i) = CK_s \left\{ 1 + \left[\left(1 + \frac{4CK_s F_i}{S_r^2} \right)^{1/2} - 1 \right]^{-1} \right\} \quad (4)$$

where f_i^* is the potential infiltration capacity as determined from Philip's equation at cell i (L/T), F_i is the cumulative infiltration at i (L), C is a parameter representing the effects of gravity, S_r is the sorptivity (LT^{-1/2}), and K_s is the surface saturated hydraulic conductivity (L/T). Both C and S_r depend on the soil texture. We assume for simplicity C to be equal to 1. To estimate S_r , we use the following relation (Dingman, 1994):

$$S_r = \left[(\phi - \theta_0) K_s |\psi| \left(\frac{2B + 3}{B + 3} \right) \right]^{1/2} \quad (5)$$

where ϕ is the soil porosity, θ_0 is the initial soil moisture, ψ is the air-entry tension (L), and B is the pore-size distribution index. The average value of these soil properties can be estimated from published data for soil textures (Dingman, 1994).

From Equation (4), the actual infiltration rate at any time during the storm is:

$$f_i = \min[f_i^*(F), P_i] \quad (6)$$

P_i is the rainfall rate at cell i (L). Infiltration excess is estimated when at a particular unsaturated cell, the condition $P_i > f_i$ is met and the amount of runoff generated at the cell is $r_i = (P_i - f_i)(1 - w_i)$ (L/T), where w_i is the impervious fraction of cell i , otherwise all the rain infiltrates provided the soil storage, S_i , is large enough.

Runoff from impervious surfaces. The assumption is made that rain falling on impervious cells immediately becomes runoff and available for routing. This assumption is reasonable in this case because most of impervious surfaces in the study area are connected to the drainage network. The runoff from impervious cells is $r_i = w_i P_i$.

The assumption that water from impervious areas does not infiltrate has a direct implication on the topographic index, which was addressed by Valeo and Moin (2001). Valeo and Moin (2001) used a modified upslope drainage area value to reflect the expected reduction in basin infiltration from the impervious cover. The modified value is estimated as $a_i' = a_i(1 - v_i)$, where v_i is the total impervious fraction upstream of a_i . Therefore, a_i' (L) is the actual pervious amount of drainage area per unit contour width upstream from cell i .

Hydrologic response

The excess rainfall is routed from hillslopes and channels using a geomorphologic instantaneous unit hydrograph (GIUH). We use a GIUH because of its simplicity and it has been shown to be useful for urbanized conditions (Olivera and Maidment, 1999; Smith *et al.*, 2005). Typically, the GIUH is expressed in terms of Strahler streams or channel links (Rodríguez-Iturbe and Valdés, 1979; Rinaldo and Rodríguez-Iturbe, 1996). In this case, we use the grid cells to obtain a GIUH described in terms of individual flow paths (Olivera and Maidment, 1999; Nicótina *et al.*, 2008). The travel time distribution, $f(t)$,

of all the paths in the basin that contribute runoff to the outlet can be expressed as follows (Saco and Kumar, 2002; D'Odorico and Rigon, 2003):

$$f(t) = \sum_{\gamma \in \Gamma} p(\gamma, t) f_{h_\gamma} \times f_{c_\gamma}(t) \quad (7)$$

where $p(\gamma, t)$ is the probability of water following path γ , Γ is the set of all possible paths, f_{h_γ} and f_{c_γ} (T⁻¹) are the probability density functions (pdfs) describing the travel times within the hillslope and channel section of path γ , respectively, and the symbol (\times) indicates the convolution operator (Saco and Kumar, 2002; D'Odorico and Rigon, 2003). To determine hillslope and channel cells, we used a fixed area threshold (Montgomery and Dietrich, 1988). For both the hillslope and channel travel time pdfs, one can assume a two-parameter inverse Gaussian (IG) distribution because of its physical basis and applicability (Rinaldo and Rodríguez-Iturbe, 1996; Olivera and Maidment, 1999; Saco and Kumar, 2002; D'Odorico and Rigon, 2003; Nicótina *et al.*, 2008). IG has the following form:

$$f_{c_\gamma}(t) = \frac{L_c}{\sqrt{4\pi D_c t^3}} \exp \left[-\frac{(L_c - u_c t)^2}{4D_c t} \right] \quad (8)$$

where L_c is the channel length (L), u_c is the kinematic wave celerity for the channel (L/T), and D_c is the coefficient of hydrodynamic dispersion for the channel (L²/T). The parameters u_c and D_c can be constant or vary depending on the path γ while L_c is always varied, this is not reflected in the notation of Equation (8) for simplicity. IG is also used for routing water from the hillslope in which case the path parameters are L_h , u_h , and D_h , and u_h and D_h can also be treated as constant or varied (Saco and Kumar, 2002; D'Odorico and Rigon, 2003; Nicótina *et al.*, 2008). The parameters L_c and L_h can be estimated from the DEM, while u_c , u_h , D_c , and D_h are normally, in practical applications, obtained from calibration (Olivera and Maidment, 1999; Nicótina *et al.*, 2008). We will refer herein to u_c and u_h as the channel and hillslope velocities, respectively.

The discharges at the outlet of the basin, $Q_i(t)$ (L/T), from the excess rain are found from the convolution of the instantaneous response, Equation (7), and the spatially averaged rate of runoff generation:

$$Q_i(t) = \sum_{\gamma \in \Gamma} \int_0^t R(\tau) \times p(\gamma, \tau) f_\gamma(t - \tau) d\tau \quad (9)$$

The subscript i indicates that $Q(t)$ can be estimated at any location of the channel network; e.g. i can be the overall basin outlet or an outlet chosen inside the overall basin. $R(t)$ is simply the total amount of runoff generated at time t in the basin divided by the total drainage area of the basin (L/T). To simplify the convolution in Equation (9), we use f_γ to represent $f_{h_\gamma} \times f_{c_\gamma}(t)$, and assume an IG distribution for f_γ (Olivera and Maidment, 1999; Saco and Kumar, 2002). The path-dependent parameters in Equation (9) are estimated in the same manner as Saco and Kumar (2002).

GIUH path probabilities and impervious surfaces. We use the term $p(\gamma, t)$ in Equation (9) to account for the effects of imperviousness in the GIUH formulation. The meaning of $p(\gamma, t)$ is the likelihood that a given path γ will carry water to the outlet and it can act as a weighting factor when summing all the possible paths Γ in the basin. In the original formulation of the GIUH, $p(\gamma, t)$ is defined in terms of Horton ratios (Rodríguez-Iturbe and Valdés, 1979; Rinaldo and Rodríguez-Iturbe, 1996). Other definitions of $p(\gamma, t)$ have been used, e.g. Woods and Sivapalan (1999) used the width function. We would like for $p(\gamma, t)$ to reflect the effects of imperviousness and rainfall variability. Therefore, we use the following expression for $p(\gamma, t)$ (Nicolina *et al.*, 2008):

$$p(\gamma, t) = \frac{r(\mathbf{x}, t)}{\int_A r(\mathbf{x}, t) d\mathbf{x}} = \frac{r(\mathbf{x}, t)}{R(t)} \quad (10)$$

We assume every cell to be a possible path. The probabilities must meet the condition $\sum_{\gamma \in \Gamma} p(\gamma, t) = 1$. $r(\mathbf{x}, t)$ is the runoff generated on cell \mathbf{x} at time t (L/T), where \mathbf{x} is a vector with the x, y location of the cell. A is the total basin area (L^2). Thus, the numerator in Equation (10) is the runoff at a given cell at time t , whereas the denominator is the total runoff in the basin at time t . $p(\gamma, t)$ is the fraction of runoff generated on a given cell. Because $p(\gamma, t)$ is defined in terms of the generated runoff, the imperviousness pattern has an effect on the likelihood of a path. Also, substituting Equation (10) into (9) simplifies Equation (9) and provides a more straightforward convolution between the path GIUH and the runoff generated at a given cell at time t , the simplified Equation (9) is:

$$Q_i(t) = \sum_{\gamma \in \Gamma} \int_0^t r(\mathbf{x}, \tau) \times f_\gamma(t - \tau) d\tau \quad (11)$$

Initial conditions

Two initial conditions are required by the chosen modelling approach: the initial average soil moisture and the initial average storage deficit in the basin. To estimate the initial average soil moisture, we used results from the analysis of seasonal soil moisture data from an urbanizing basin located in close proximity to our study area (Tenenbaum *et al.*, 2006). The basin studied by Tenenbaum *et al.* (2006) has similar underlying geology, soils, and imperviousness to our study area.

To estimate the initial average storage deficit, the method proposed by Troch *et al.* (1994) was tried. However, the Troch *et al.* (1994) method requires a specific form for the recession hydrograph that does not conform well to the recessions observed in our study area. Another drawback of this method within our application is the need to add another initial condition, the drainable porosity, to convert an initial depth to an initial storage. Hence, we treat the initial deficit as a parameter that needs to be calibrated.

Baseflow separation

An expression for the baseflow discharge at the basin outlet can be derived from the topographic index and the average storage deficit (Duan and Miller, 1997). Instead of using this expression, we use the streamflow data to estimate the baseflow discharge following the method of Brutsaert and Nieber (1977) and the extension proposed by Szilagyi and Parlange (1998). We believe a lumped approach to baseflow contributions is acceptable in this case, given the few data available about groundwater dynamics in the study area, and because our emphasis is on the effects of imperviousness on surface flow.

The method proposed by Brutsaert and Nieber (1977) and Szilagyi and Parlange (1998) assumes the following relation holds for the recession part of the streamflow hydrograph:

$$\frac{dQ(t)}{dt} = -bQ(t)^c \quad (12)$$

where b and c are fitting parameters. The details about the exact way in which the separation is done are described in Szilagyi and Parlange (1998), and therefore are omitted from this description.

STUDY AREA

For this study, a sub-urban basin located within the Northwest Branch Anacostia River basin (NW Branch basin), in the State of Maryland, USA, was selected. The map in Figure 1 illustrates the location of the NW Branch basin within Maryland, together with the stream network, the imperviousness pattern, and the two U.S. Geological Survey (USGS) streamflow gages. The basin has a total drainage area of 124 km² and a total imperviousness of 17%. The basin extends into Montgomery and Prince George's counties in Maryland and joins downstream the Potomac River within the Washington D.C. boundaries. The basin has a tidal portion mostly located within Washington D.C. We limit our study to the non-tidal portion of the basin.

The NW Branch basin was selected mainly because it has a characteristic sub-urban pattern (mixed pervious-impervious land use) and an imperviousness gradient. The gradient consists of imperviousness accumulating as one moves from the most upstream areas in the basin, farthest from the overall outlet, to the main basin outlet as illustrated in Figure 1. The NW Branch basin has two locations where USGS streamflow measurements are available. The USGS gage number 01651000 is located at the overall outlet of the NW Branch basin and drains an area of 124 km² out of which 17% is impervious. This gage and its drainage area are referred herein as HG because the gage is located near the town of Hyattsville, Maryland. The USGS gage number 01650500 in Figure 1 drains an area of 54 km² out of which 7% is impervious. This internal gage and its sub-basin are referred herein as CG because the gage is located near the town of Colesville, Maryland. There is no rain gage data available within the basin, we

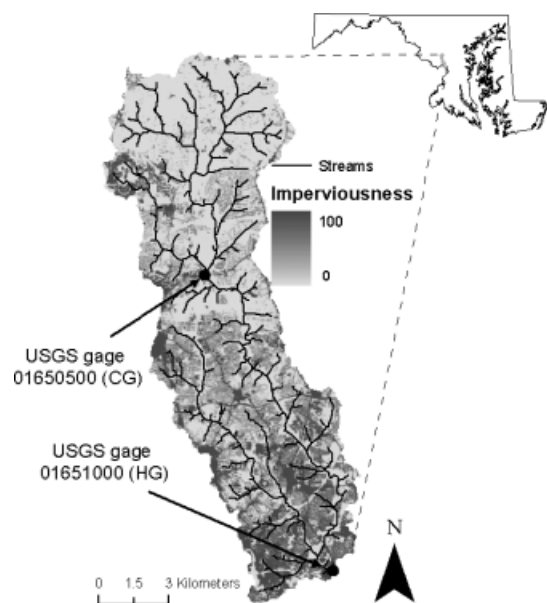


Figure 1. Map illustrating the location of the NW Branch basin within the State of Maryland, USA. The basin map illustrates the stream network derived from DEM data, the imperviousness pattern, and the two locations where USGS streamflow data are available

used instead Next Generation Weather Radar (NEXRAD) stage III rainfall data (National Oceanic and Atmospheric Administration, 2008a). The climate in the basin is humid temperate with an annual wetness index of approximately 1.4 (Tenenbaum *et al.*, 2006). The physiography of the basin is described by the Piedmont Plateau region. The Piedmont is characterized by rolling hilly terrain conformed by a well-defined system of ridges, hills and valleys, and shallow soils (Miller *et al.*, 2007). The land cover consists mostly of sub-urban and grassland areas. A small amount of commercial and cultivated crop cover is also present. The percentages of the main aggregated land cover classes are approximately 60% urban and sub-urban development, 29% forest and grasslands, and 11% of cultivated crop areas.

DATA SETS

For the input or forcing data, we used NEXRAD stage III radar rainfall at the 1-h time resolution and at approximately 4 km spatial resolution (National Oceanic and Atmospheric Administration, 2008a). The stage III radar data was used not only because of the lack of gaged data but also because the spatial distribution of rainfall is known to be particularly important in urbanized basins (Smith *et al.*, 2005; Segond *et al.*, 2007). Since the imperviousness data used depicts conditions in the year 2001, we selected storm and streamflow data between the 1999 and 2001 time period, where land-use conditions can be assumed to be approximately stationary. The 1999–2001 time window also matches the period where both radar rainfall and higher resolution streamflow data are available for HG and CG. Six well-documented storms were carefully selected with the help of the U.S. National Climatic Data Center (NCDC) Storm Event

Table I. Characteristics of the storm events selected for this study

Storm	Depth (cm)	Maximum intensity (cm/h)	Duration (h)	COV ^a	Recurrence interval ^b
21 March 1999 ^c	2.17	1.71	8	0.22	1.5
25 August 1999	1.67	0.90	7	0.12	1
21 March 2000 ^c	2.21	1.17	12	0.18	1
17 April 2000 ^c	2.17	0.80	12	0.12	1
29 March 2001	0.95	0.64	8	0.066	<1
4 July 2001 ^c	2.57	1.58	8	0.38	4

^a Coefficient of variation from the accumulated rainfall amounts at every grid cell.

^b Estimated from NOAA Atlas 14 (National Oceanic and Atmospheric Administration, 2008c).

^c Storms selected for calibration in the split sample test, the remaining two storms were used for evaluation.

Database (National Oceanic and Atmospheric Administration, 2008b). The storms and their characteristics are shown in Table I. Using the NCDC Storm Event Database, the storms were selected to have caused soil saturation during the event and to represent average rainfall conditions, as opposed to extreme conditions where severe flooding is recorded. The streamflow data needed for the gages at HG and CG were obtained from the USGS Instantaneous Data Archive at the 15-min resolution (U.S. Geological Survey, 2008a). To match the spatial resolution of the imperviousness data, the rainfall radar data were interpolated using an inverse distance squared weighting method.

The DEM and imperviousness data were obtained from the USGS at a resolution of approximately 30 m (U.S. Geological Survey, 2008b,c). To preserve the resolution of both of these data sets, this same spatial resolution was used in the model for the partitioning of rainfall and routing of runoff. The DEM was used to determine the area draining to each cell, the D ∞ and D8 flow directions, and the stream network (Tarboton, 1997). The D ∞ flow directions were used in estimating the topographic index because this approach can more realistically reproduce the drainage tendencies of hillslopes (Tarboton, 1997). The D8 flow directions were used to route the generated runoff and avoid having multiple flow routing paths for hillslope cells. The stream network was derived using a fixed area threshold (Montgomery and Dietrich, 1988). The threshold used was 0.2 km², which compares well with blue lines from the 1:100k NHDPlus hydrography data set of the U.S. Environmental Protection Agency (EPA) (U.S. Environmental Protection Agency and U.S. Geological Survey, 2006). The imperviousness data consists of the fraction of imperviousness at every cell in a grid derived from remotely sensed data (Homer *et al.*, 2007). We will refer herein to the imperviousness fraction of a cell as the local imperviousness. The soil data was obtained from the U.S. Natural Resources Conservation Service (NRCS). Both SSURGO (Natural Resources Conservation Service, 2008a) and STATSGO (Natural Resources Conservation Service, 2008b) data were used,

since the higher resolution SSURGO data were not available for the entire study area. However, after classifying soils in the study area according to soil textures, it was found that soils are highly homogeneous and characterized by a single soil class, silt-loam. The soil parameters associated with silt-loam soils were obtained from the literature (Dingman, 1994), and their values are $K_s = 2.59$ cm/h, $\phi = 0.485$, $\psi = 78.6$ cm, and $B = 5.30$. The soil parameters are needed to estimate the infiltration capacity at the soil surface, and they are used in the estimation of Equations (4) and (5). All data were projected and put into a consistent system of the Maryland State Plane (Stern, 1990).

RESULTS AND DISCUSSION

The results from applying the event model are divided into three sections. In the first section, the event model is assessed using a split sample test and parameter sensitivity analysis. The assessment is not intended to be an exhaustive one, since other authors have previously evaluated the modelling concepts used (Olivera and Maidment, 1999; Valeo and Moin, 2001). In the second and third sections, the event model is used to investigate the role of the imperviousness gradient and pattern. In the second section, the storm hydrographs at various internal locations in the basin are compared. The third section compares the changes in the hydrologic response from various imperviousness scenarios.

Assessment of modelling approach

We performed a model calibration to determine suitable values for the parameters S_{\max} , u_h , u_c , D_c , and D_h , and the initial condition \bar{S} ; the calibration was also done to better understand the behaviour of parameters and to identify limitations in the modelling approach. The soil parameters in Equations (4) and (5) were assumed to be equal to their average value and constant for all the simulations. We assumed for the calibrations different parameter sets for the two basins where streamflow data are available, HG and CG, and for each of the four storms identified in Table I. The calibrations were performed in three steps. The first step was to manually adjust parameters and choose the form of the transmissivity profile. In the second step, the Generalized Likelihood Uncertainty Estimation (GLUE) method was used to investigate the identifiability and sensitivity of parameters (Beven and Binley, 1992). In the third step, a parameter set was chosen using the results from the manual calibrations and sensitivity analysis. The goodness-of-fit of simulations was quantified using the Nash Sutcliffe (NS) coefficient (Nash and Sutcliffe, 1970) and the modified correlation coefficient (R_{mod}) (McCuen and Snyder, 1975).

Choosing the form of the transmissivity profile is the equivalent of deciding the value of n in Equations (1) and (3) (Duan and Miller, 1997). A preference for larger values of n was observed in the calibrations and because from the baseflow separation the recession exponent c in

Equation (12) was found to be approximately equal to 2, the exponential transmissivity profile was chosen for all the simulations (Duan and Miller, 1997). The relationship between n and other model parameters was not explored further. Such an investigation would need to include more specific soil profile data than was available in this study. Another simplification made was to ignore the imperviousness when estimating the topographic index. We found the calibration results to be essentially the same when we did not account for the reduction in upslope contributing area due to imperviousness, a similar result was found by Valeo and Moin (2001). This lack of sensitivity of the topographic index at the basin-wide scale was described and discussed in detail by Franchini *et al.* (1996).

For the identifiability and sensitivity analysis, we used the version of GLUE in the Monte-Carlo Analysis Toolbox (MCAT) (Beven and Binley, 1992; Wagener *et al.*, 2004). For each behavioural parameter set Θ_j , we used the NS coefficient to find the normalized pseudo-likelihood function, $L(\Theta_j)$, which can be defined as:

$$L(\Theta_i|Y) = \frac{NS_i}{\sum_{i=1}^M NS_i} \quad (13)$$

where Y are the streamflow observations and M is the number of behavioural sets selected from the Monte-Carlo realizations. Figure 2 shows the scattergram obtained from 10 000 model simulations and a single storm event; using the criteria $NS > 0.8$ to select the behavioural set, analogous scattergrams were found for the other storms. It is evident in the scattergram that the channel velocity is very sensitive and well identified, while the other parameters are less identifiable. The regional sensitivity analysis, as implemented in MCAT (Wagener *et al.*, 2004), indicated the channel velocity to be the most sensitive parameter, while the other parameters were relatively less sensitive with D_h being the most insensitive. The Kolmogorov–Smirnov (KS) test comparing the behavioural set pdf of each parameter to a uniform pdf bounded by the parameter range indicated all parameters to be sensitive except D_h . The estimated KS statistic d for D_h was less than d_{\max} ($d_{\max} = 0.13$ at the 0.005 level of significance) for all the storms, while the other parameters had d values greater than d_{\max} . The apparent lack of identifiability in Figure 2 can be explained by including in the scattergram plots the initial condition and the combined hillslope and channel travel times. Thus, the scattergram for the initial value of the ratio \bar{S}/S_{\max} , $E(\delta)$, the mean travel time, $E[f(t)]$, and the variance of the travel times, $var[f(t)]$, was determined and is shown in Figure 3. The initial $E(\delta)$ has the role of deciding the degree of soil saturation in the basin just before the rain starts, and thus its identifiability is more relevant in this case than S_{\max} alone. Similarly, for the routing parameters, $E[f(t)]$ and $var[f(t)]$ ultimately define the form of the GIUH (Rinaldo and Rodríguez-Iturbe, 1996; Nicótina *et al.*, 2008). $E[f(t)]$ and $var[f(t)]$ were found using the

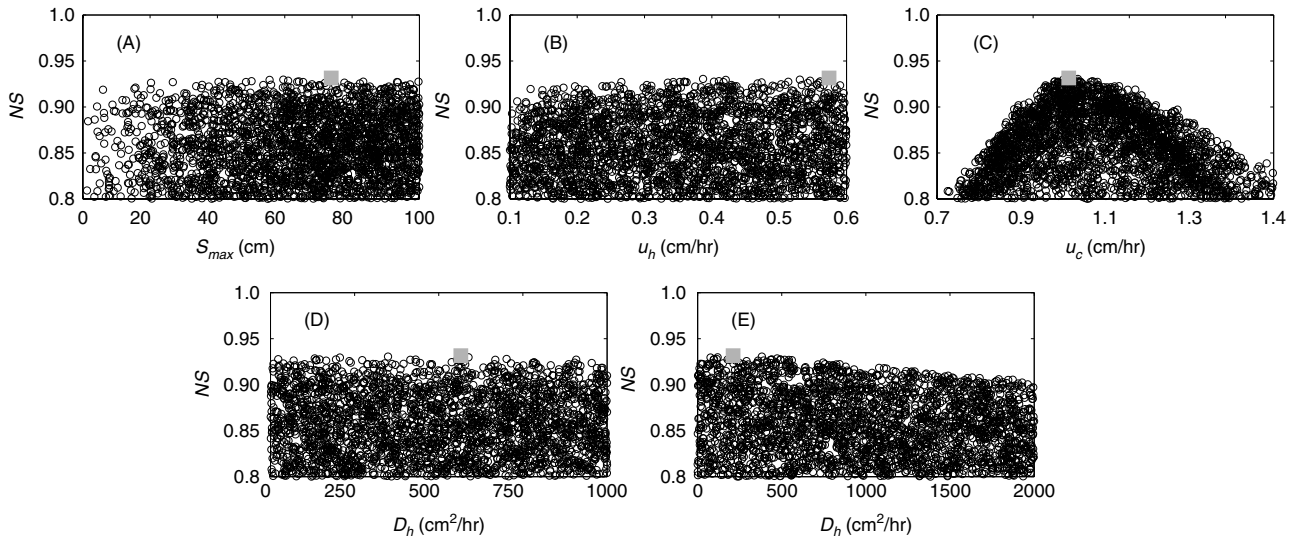


Figure 2. Scattergram obtained from 10 000 Monte-Carlo simulations and the 21 March 2000, storm event, for the five parameters in the model: (a) S_{max} , (b) u_h , (c) u_c , (d) D_h , and (e) D_c . Each dot in the plots is a simulation with parameter values sampled from a uniform pdf. The bounds of the pdfs were the same as the ranges shown for the x-axis above. Only the simulations that met the condition $NS > 0.8$ are shown. The solution with the highest NS value is indicated by the square symbol

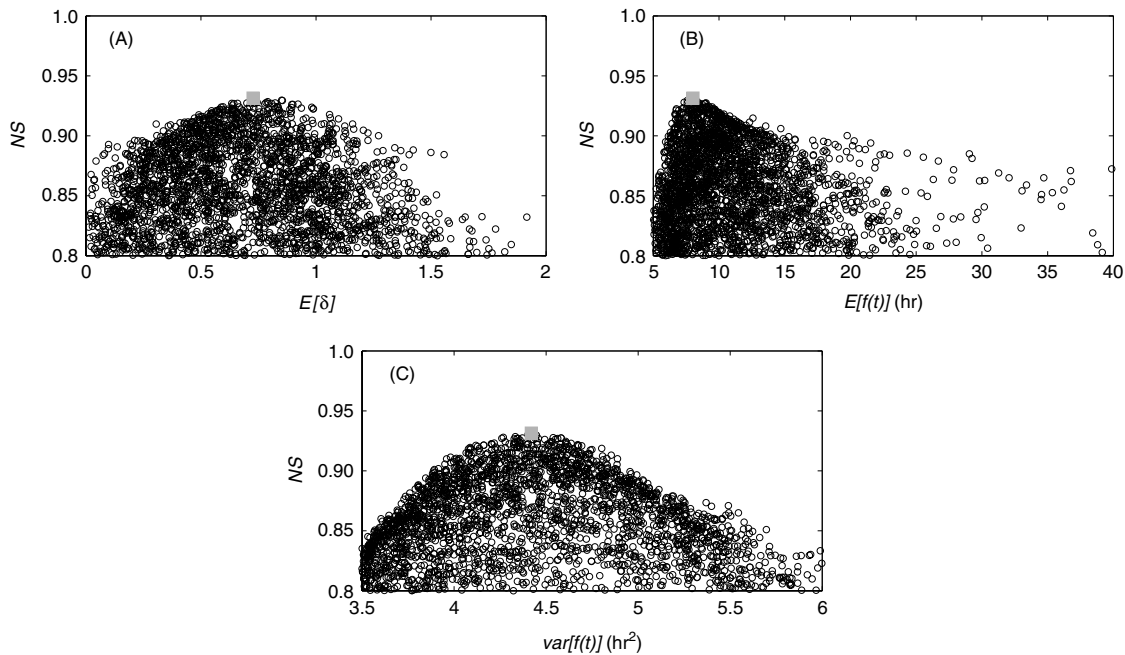


Figure 3. Scattergram obtained from 10 000 Monte-Carlo simulations and the 21 March 2000, storm event, for the (a) initial ratio of \bar{S}/S_{max} , $E(\delta)$, (b) the mean travel time $E[f(t)]$, and (c) the variance of the travel times, $var[f(t)]$. Each dot in the plots is a simulation run with parameter values (the five parameters in the model) sampled from a uniform pdf. Only the simulations that met the condition $NS > 0.8$ are shown. The solution with the highest NS value is indicated by the square symbol

expression of Saco and Kumar (2002) and by integrating the time in Equation (10) to obtain $p(\gamma)$. Figure 3 shows the parameters are more identifiable when the initial condition, \bar{S} , and the maximum storage deficit, S_{max} , are treated as a single parameter, and when the hillslope and channel parameters are considered together.

The split sample test resulted in different parameter values for each of the four storms used in the calibration, these values were averaged to obtain a single parameter set for HG and CG. This parameter set is shown in Table II. Table II shows a consistent value of S_{max} for HG and CG, while the routing parameters varied

Table II. Single parameter set found from the calibration of four storms. The single parameter set was obtained by averaging the parameter values obtained for each of the four calibrated storms

Basin	S_{max} (cm)	u_h (m/s)	u_c (m/s)	D_h (m ² /s)	D_c (m ² /s)
HG	50	0.55	0.90	100	200
CG	50	0.40	0.80	300	500

between the two basins, the velocities increased with drainage area, and the dispersions decreased. This scale dependency of the routing parameters was expected as supported by empirical studies (Leopold and Maddock,

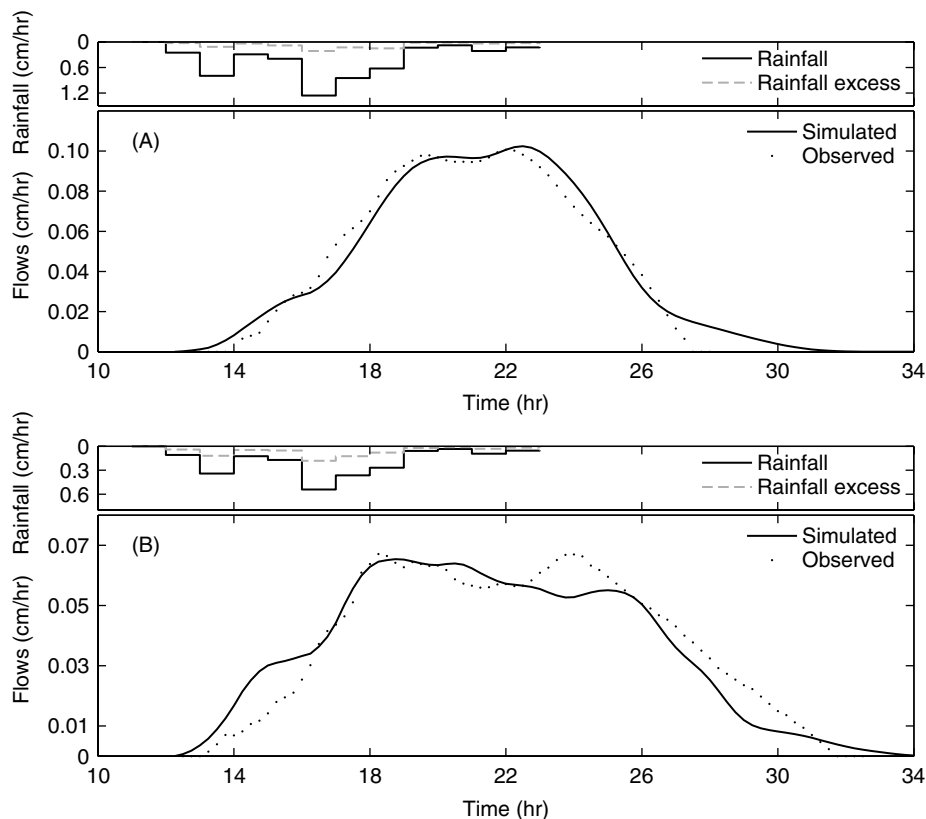


Figure 4. Calibration results for the 21 March 2000, storm event at HG and CG. Observed and simulated flows at (a) CG and (b) HG. The rainfall and rainfall excess are the areal averaged values obtained from the radar rainfall data and the spatially simulated runoff, respectively. The areal averaged rainfall and rainfall excess are only shown for illustrative purposes, they were not used directly in the simulations

1953). Figure 4 shows the final calibration results for the 21 March 2000, storm event for HG and CG. Figure 4a shows the calibration results for CG, the NS and R_{mod} values for this calibration are 0.96 and 0.95, respectively. Figure 4b shows the results for HG, in this case the NS and R_{mod} values are 0.91 and 0.90, respectively. Overall, the calibrated results performed reasonably well, but when a single parameter set was used to perform the evaluation, the goodness-of-fit coefficients decreased. The NS coefficient decreased on average by 22% and R_{mod} by 19%. The hydrographs estimated for the two storms used in the evaluation are shown in Figures 5 and 6. In general, we found the simple event model has a better ability to predict peak flows than other parts of the hydrograph. Table III summarizes the NS , R_{mod} , and the difference between the observed and simulated peak flow and time to peak for the calibration and evaluation events.

Some of the limitations of the modelling approach are visible in Figure 6. The overestimation of observed flows on the rising limb of the hydrographs in Figure 6a and b suggests areas where the model structure could be improved. The overestimation is likely due in part to the unaccounted effects of initial rainfall storage on localized depressions, and uncertainty in the estimate of the initial condition \bar{S} . We used an average calibrated value for \bar{S} that changed for spring and summer flows, but a tendency for \bar{S} to vary within seasons was observed. The storm dependency of routing parameters was a minor concern in

Table III. Summary of NS , R_{mod} , absolute difference between observed and simulated peak flows, and absolute difference between observed and simulated time to peak for the calibration and evaluation events

Basin	Storm	NS	R_{mod}	ΔQ_p^a (%)	ΔT_p^b (%)
Hyattsville (HG)	21 March 1999 ^c	0.57	0.46	8.3	1.9
	25 August 1999	0.74	0.55	4.2	2.2
	21 March 2000 ^c	0.91	0.9	3.3	2.8
	17 April 2000 ^c	0.78	0.69	3.4	6.1
	29 March 2001	0.57	0.65	1.9	3.3
Colesville (CG)	4 July 2001 ^c	0.42	0.36	13	26
	21 March 1999 ^c	0.63	0.79	10	14.3
	25 August 1999	0.58	0.69	8	4.3
	21 March 2000 ^c	0.96	0.95	5.9	9.1
	17 April 2000 ^c	0.45	0.33	25	8.7
	29 March 2001	0.64	0.61	12.5	3.1
4 July 2001 ^c	0.9	0.73	4	3.7	

^a Absolute percent difference between the observed and simulated peak flow.

^b Absolute percent difference between the observed and simulated time to peak.

^c Storms selected for the calibration in the split sample test.

this case, because we selected average rainfall conditions and storms with similar return periods. However, during calibration we found u_c to range from 0.78 to 1.28 m/s, instead of having a single value. For instance, in Figure 2, if u_c is chosen to be 0.7 instead of the optimum value of 0.96, the NS coefficient decreases by approximately

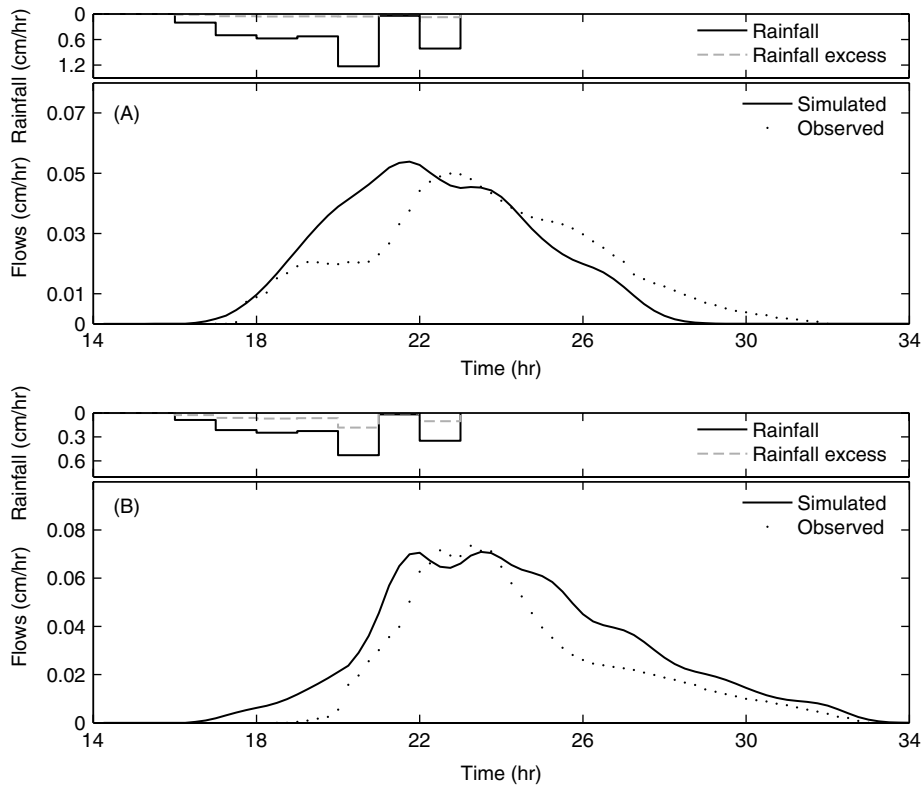


Figure 5. Evaluation results for the 25 August 1999, storm event at HG and CG. Observed and simulated flows at (a) CG and (b) HG. The rainfall and rainfall excess are the areal averaged values obtained from the radar rainfall data and the spatially simulated runoff, respectively. The areal averaged rainfall and rainfall excess are only shown for illustrative purposes, they were not used directly in the simulations

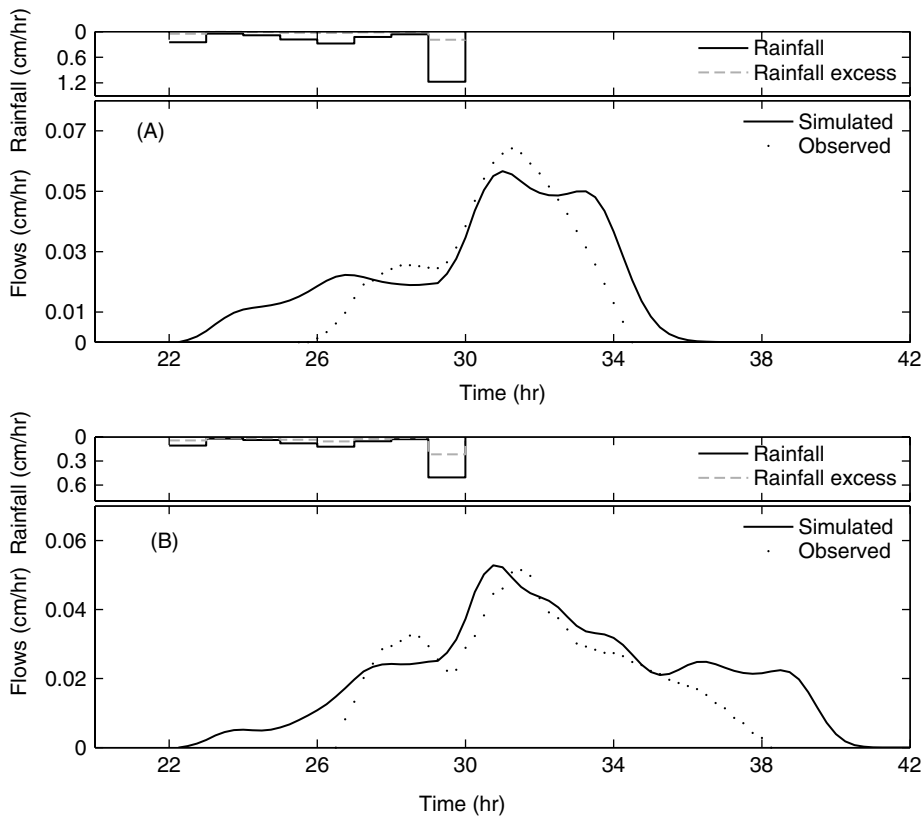


Figure 6. Evaluation results for the 29 March 2001, storm event at HG and CG. Observed and simulated flows at (a) CG and (b) HG. The rainfall and rainfall excess are the areal averaged values obtained from the radar rainfall data and the spatially simulated runoff, respectively. The areal averaged rainfall and rainfall excess are only shown for illustrative purposes, they were not used directly in the simulations

25%. The storm dependency of u_c , or its time-variant character, was somewhat expected, since it was present in the original formulation of the GIUH (Rodríguez-Iturbe and Valdés, 1979).

Effects of the imperviousness gradient

For the remainder of the analysis, we focus on the 21 March 2000, storm event shown in Figure 4. This storm event is characteristic of average rainfall conditions in our study area. The objective is to use this storm event to perform a series of comparisons and to further investigate the role of imperviousness. We will try to account for the scale dependency of the routing parameters but assume they are time invariant throughout the storm. We are more interested in the spatial variation of the routing parameters, in particular the velocities, because their scale dependency makes it difficult to explore the role of imperviousness at internal locations in the basin. We will emphasize in the next comparisons of peak flows and the time to peak since the assumption of time-invariant velocities is more suitable for estimating peak flows (Rodríguez-Iturbe and Valdés, 1979). To estimate the velocity field, we propose the use of a Leopold–Maddock type parameterization for channel velocities (Leopold and Maddock, 1953). The proposed parameterization is as follows:

$$u_i \propto A_i^\alpha I_i^\beta \quad (14)$$

where u_i (L/T) is the velocity at location i , A is the drainage area at i (L^2), and I is the total imperviousness upstream of location i . The proportionality constant and the exponents α and β in Equation (14) were estimated by calibration. We found the proportionality constant in Equation (14) to be equal to 0.37 m/s, $\alpha = 0.04$, and

$\beta = 0.15$. The value of α compares well with empirical values (Leopold and Maddock, 1953).

In addition, a similar mathematical relation to Equation (14) was found for peak flows of a given return period for gaged urban basins in the Maryland Piedmont (Moglen *et al.*, 2006). Equation (14) is also written in terms of imperviousness to identify the dependency of u on imperviousness. For the dispersion, the following parameterization is used:

$$D_i \propto u_i \quad (15)$$

where the proportionality constant was found by calibration to be equal to 272 m^2/s . The parameterization for the dispersion was kept simpler because there is little empirical evidence about its scaling with drainage area (Toprak and Cigizoglu, 2008).

To evaluate the calibrated parameters for Equations (14) and (15), we performed a simplified version of the proxy-basin test (Ewen and Parkin, 1996). The proxy-basin test performed consisted of using the CG basin for calibration and the HG basin for evaluation. Figure 7 shows the results of this simplified version of the proxy-basin test. The NS and R_{mod} for the calibration, Figure 7a, are 0.92 and 0.94, respectively. For the evaluation, Figure 7b, the NS and R_{mod} are 0.82 and 0.90, respectively. In Figure 7, the model shows a reasonable ability to match peak flows, as expected from the assumption of time-invariant velocities, but a tendency to overestimate the recession flows in the case of HG and underestimate in the case of CG. The calibrated model with the spatially varying velocities and dispersions was used to investigate the role of the imperviousness gradient by selecting and comparing four internal sub-basins.

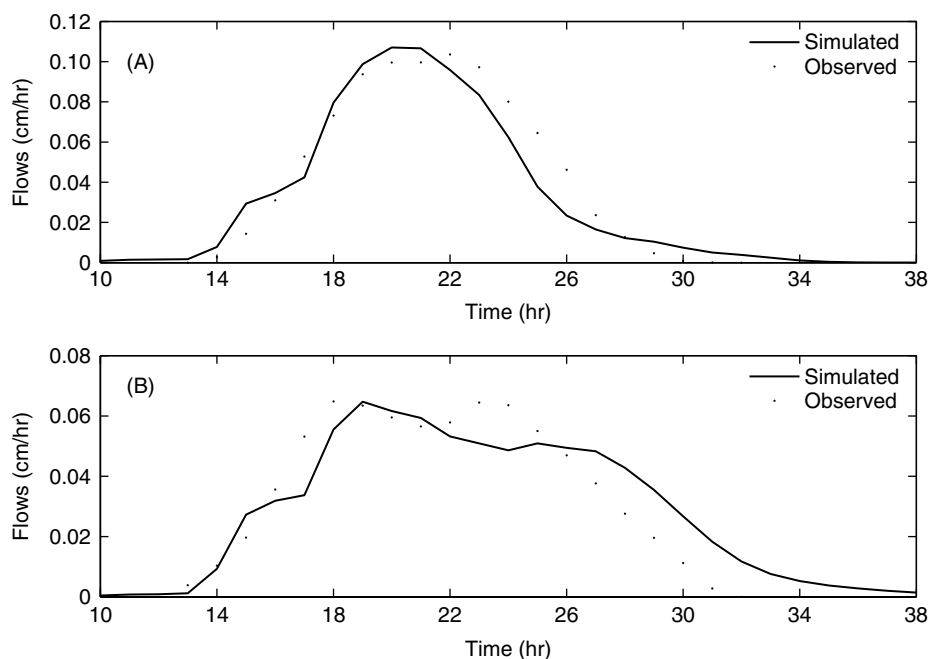


Figure 7. Results from the simplified proxy-basin test used for the calibration–evaluation of the spatially distributed routing parameters. (a) Calibration based on the CG streamflows and (b) evaluation based on the HG streamflows, for the 21 March 2000, storm event

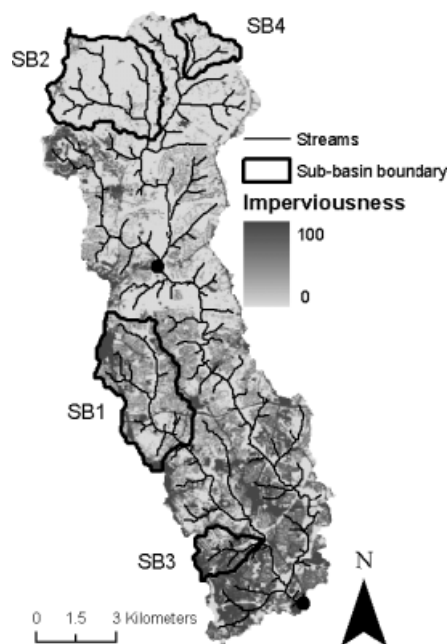


Figure 8. Sub-basin chosen to investigate the role of the imperviousness gradient on the hydrologic response. The pair SB1–SB2 each has a drainage area of approximately 12.6 km² and total imperviousness of 24.5 and 2.5%, respectively. The pair SB3–SB4 each has a drainage area of approximately 2.9 km² and total imperviousness of 37.7 and 3.5%, respectively

Table IV. Drainage area and total imperviousness of the sub-basins selected to examine the role of the imperviousness gradient. The pairs SB1–SB2 and SB3–SB4 are used together in the comparisons

Sub-basin	Drainage area (km ²)	Imperviousness (%)
SB1	12.58	24.5
SB2	12.63	2.5
SB3	2.93	37.7
SB4	2.97	3.5

The selected sub-basins are shown in Figure 8. The sub-basins were selected to constitute two pairs of basins with approximately the same drainage area but strikingly different levels of imperviousness (Table IV). For the pair SB1 and SB2, the hydrographs obtained for the 21 March 2000, storm are shown in Figure 9a. In this figure, the peak flow for SB1 is 20% larger than SB2, the sub-basin with greater imperviousness has the largest peak as one might expect. However, the opposite is the case for SB3 and SB4 (Figure 9b). This figure shows that the peak flow for SB4 is 25% larger than for SB3, although SB4 has a much lower amount of total imperviousness than SB3. SB4 is only 3.5% impervious while SB3 is 37.7%. The reason for this is the uneven distribution of rainfall and runoff for the storm of 21 March 2000. The rainfall amounts are greater on the upper portions of the basin than near the main outlet. No differences in the time to peak were observed in Figure 9a and b. The same comparison just performed was repeated assuming spatially uniform rainfall, this emphasizes the role of imperviousness by removing the

effects of spatially variable rainfall. The uniform rainfall was obtained from the areal average of the radar rainfall. The model was recalibrated using the simple proxy-basin test previously described. The NS coefficient and R_{mod} for the recalibration were 0.94 and 0.87, respectively, and 0.78 and 0.79 for the evaluation, respectively. The results from the uniform rainfall assumption are consistent with the general observation of increasing peak flows with increasing imperviousness as illustrated in Figure 9c and d. In Figure 9c, the peak flow increased by 28% and in Figure 9d by 18%, in both cases the sub-basin with the largest imperviousness, SB1 and SB3, produced the largest peak flow. The results suggest that the interaction between the spatiotemporal variability of rainfall and the imperviousness pattern can result in hydrologic behaviour, e.g. higher peak flows in less urbanized portions of the basin, that is more complex than generally recognized. This can be a relevant consideration when trying to develop simple peak flow models, such as urban regression equations in urbanized basins.

Effects of the imperviousness pattern

The previous comparison between sub-basins could be extended to analyse the role of the imperviousness pattern by selecting a pair of sub-basins with the same drainage area and amount of imperviousness, but contrastingly different development patterns. Unfortunately, the HG sub-basins that meet this criterion have relatively small drainage areas, where the effect of hillslope routing could be dominant and difficult to identify. Instead, we used simulated imperviousness patterns. The patterns were simulated using a similar methodology to the one described in Mejia and Moglen (2009), and they typify extreme ways of organizing imperviousness in the basin. Figure 10 illustrates the three patterns that were used. The pattern in Figure 10a is the actual National Land Cover Database (NLCD) imperviousness pattern (current scenario). The patterns in Figure 10b and c represent different ways of clustering imperviousness. Figure 10b has the advantage of reducing peak flows along the channel network, while Figure 10c will tend to increase peak flows but at the same time it steers development away from the floodplains (Mejia and Moglen, 2009). The pattern in Figure 10b is referred herein as the channel clustering scenario and the one in Figure 10c as the source clustering scenario. The way in which the channel clustering and source clustering scenarios tend to decrease and increase, respectively, peak flows globally, along the entire stream network, is described in Mejia and Moglen (2009). Figure 10d shows uniformly distributed imperviousness in the basin, this pattern is mimicking an extreme case of urban sprawl and it is referred herein as the uniform scenario. It is important to mention that all the scenarios maintain the total imperviousness and the distribution of local imperviousness in the overall basin at the same level as the current scenario, with only the spatial organization being changed.

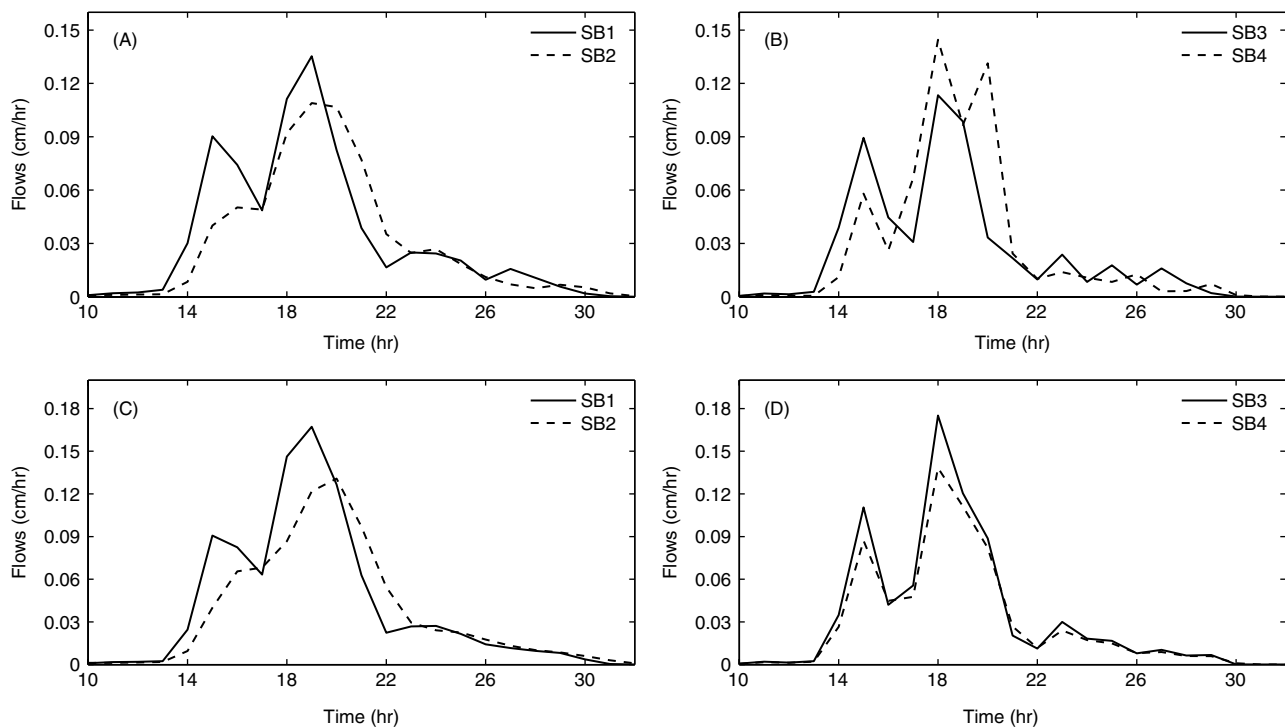


Figure 9. Comparison of simulated hydrographs for the selected sub-basins. (a) Comparison for the pair SB1–SB2 and (b) SB3–SB4 using spatially distributed rainfall. (c) Comparison for the pair SB1–SB2 and (d) SB3–SB4 using uniform rainfall. The pair SB3–SB4 each has a drainage area of approximately 2.9 km², while SB1–SB2 each is approximately 12.6 km²

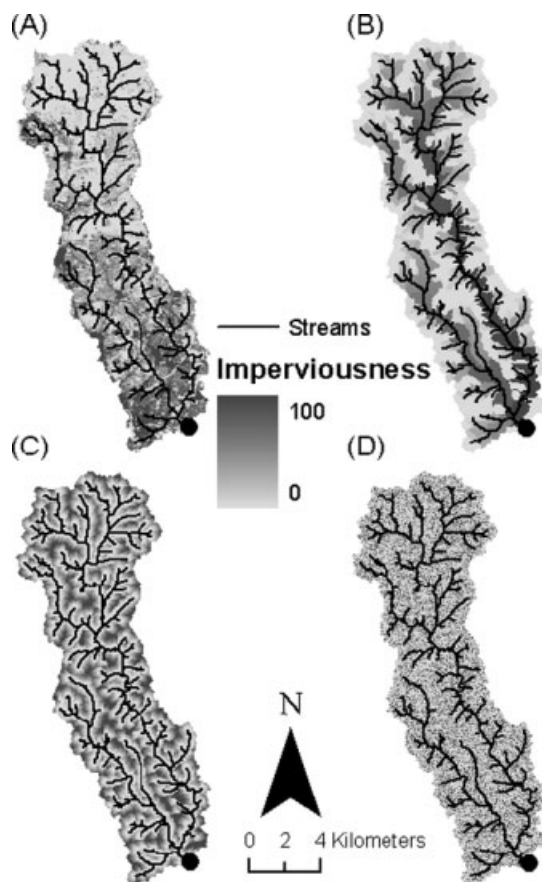


Figure 10. Current and simulated imperviousness patterns used for the comparison of scenarios: (a) current scenario, (b) channel clustering scenario, (c) source clustering scenario, and (d) uniform scenario

Figures 11 and 12 show the simulation results for HG and CG, respectively, from assuming the various imperviousness scenarios. The figures also show the uncertainty bounds estimated using the Shuffled Complex Evolution Metropolis (SCEM) algorithm and GLUE (Beven and Binley, 1992; Vrugt *et al.*, 2003). The bounds are included to help distinguish the changes in the hydrograph that are due to the imperviousness scenarios from those due to variability in the parameters and initial condition. In Figure 11, the peak flow relative to the simulated peak flow for the current scenario decreased by 6% (Figure 11b), 1% (Figure 11c), and 4% (Figure 11d) for the channel clustering, source clustering, and uniform scenarios, respectively. The most substantial change was a delay in the time to peak of approximately 4 h for both the source clustering and uniform scenarios. In both scenarios, the change in the peak flow and time to peak is outside the SCEM and GLUE estimated bounds, indicating the change is bigger than the variability associated with parameters and the initial condition. Thus, the impact of the patterns on the hydrologic response can be significant. The opposite trend is observed in Figure 12 for CG, the time to peak did not change but the peak flow increased relative to the current scenario by 18% (Figure 12b), 30% (Figure 12c), and 27% (Figure 12d) for the channel clustering, source clustering, and uniform scenarios, respectively. The increases in peak flow are all outside the estimated bounds indicating that the increases can be significant, although the increases are, in part, due to increases in the total imperviousness in CG.

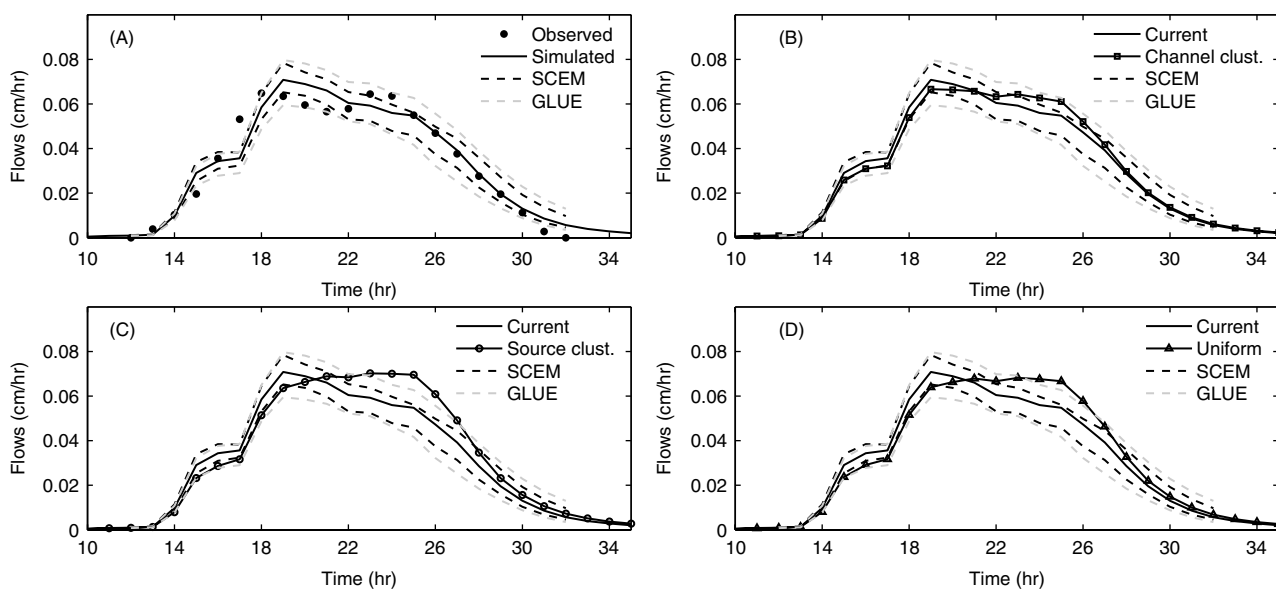


Figure 11. Comparison of the hydrographs obtained from the imperviousness scenarios at HG, including the 95% uncertainty bounds associated with the parameters and the initial condition. (a) Observed flows and current scenario, (b) current and channel clustering scenarios, (c) current and source clustering scenarios, and (d) current and uniform scenarios

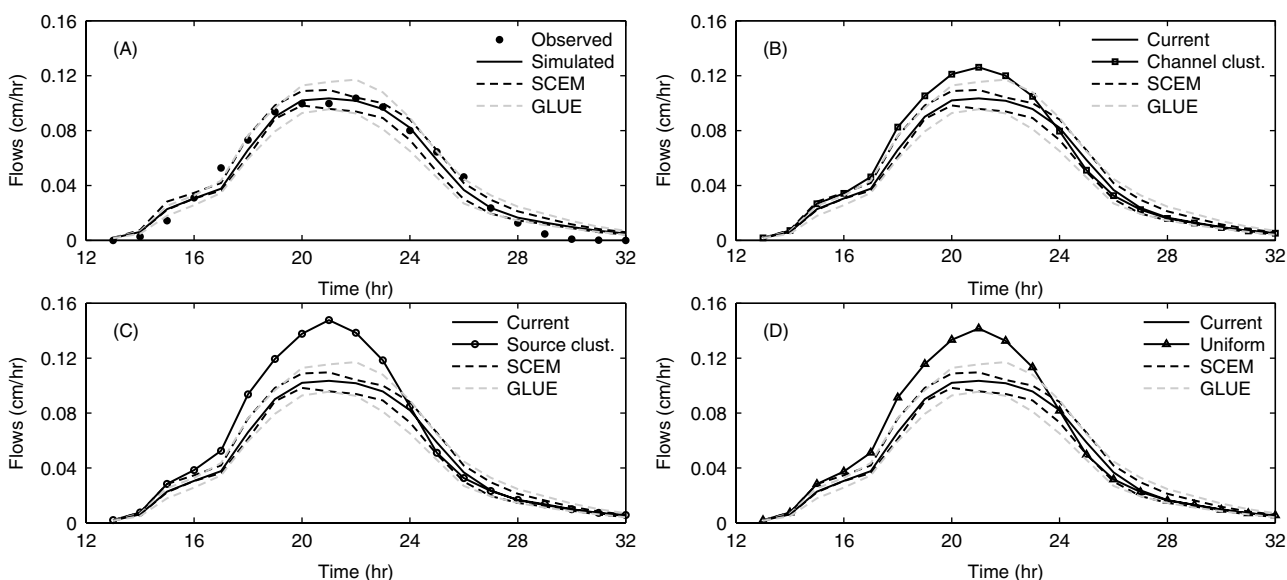


Figure 12. Comparison of the hydrographs obtained from the imperviousness scenarios at CG, including the 95% uncertainty bounds associated with the parameters and the initial condition. (a) Observed flows and current scenario, (b) current and channel clustering scenarios, (c) current and source clustering scenarios, and (d) current and uniform scenarios

The main reason for the decrease in peak flows at the outlet of HG from the channel clustering, source clustering, and uniform scenarios is because the current scenario tends to concentrate imperviousness near the main outlet. This can allow the current scenario to produce a faster response and higher peak flows at the main outlet. However, when HG is compared to conditions at an interior location in the basin (CG), the peak flows from the channel clustering, source clustering, and uniform scenarios can be substantially larger than in the current scenario. The point we want to emphasize here is that the way imperviousness is organized on the landscape can influence the magnitude of the impact (i.e. increases in peak flows). Further, quantifying the change in peak flows at

a single location (outlet) could undermine a larger effect within the basin, and this appears in part dependent upon the coincidence between the spatiotemporal variability of rainfall and the imperviousness pattern. In summary, the imperviousness pattern can produce significant impacts on the hydrologic response at the overall outlet as well as at internal locations. The impacts at internal locations can be amplified by the large-scale re-ordering of imperviousness locations produced by the various patterns.

CONCLUSIONS

We applied an event model to an urbanizing basin, by making several simplifying assumptions about the effects

of imperviousness. We started by assuming a sub-urban basin where the land use is characterized by both pervious and impervious conditions. To model pervious conditions, we used a topographic index and Philip's infiltration equation to account for both saturation and infiltration excess, respectively (Philip, 1960; Beven and Kirkby, 1979; Troch *et al.*, 1994). To model imperviousness, we assumed rain falling on impervious cells becomes runoff because most of the impervious surfaces in the basin are directly connected to the drainage network. We used a geomorphic unit hydrograph for routing all the runoff (Rodríguez-Iturbe and Valdés, 1979; Rinaldo and Rodríguez-Iturbe, 1996), and assumed the effects of imperviousness on surface flows could be represented by a time-invariant velocity field (Olivera and Maidment, 1999).

The assessment of model parameters showed the channel velocity to be very sensitive and an important parameter in estimating the hydrologic response of an urbanized basin. Effort in the direction of a more general representation of channel routing, e.g. time-variant parameters, appears promising at improving predictions under urbanized conditions. It is likely that the sensitivity of channel routing parameters is enhanced by the stormwater system, which links rainfall directly to the channel routing process without the modulating effect of hillslope processes. This then reinforces the need for accurate estimates of the spatial pattern of rainfall, as connected imperviousness can increase the role of spatial variability in the rainfall on the hydrologic response. The comparison of internal sub-basins revealed an interesting fact about the urban land-use condition. The coincidence of higher rainfall intensity on the most pervious portion of the basin led to higher peak flow in these areas than the most urbanized ones. Conventional wisdom holds that higher imperviousness leads to higher peak flows. This general perception seems to hold, at least in our case, when rainfall is assumed uniform and some of the interactions between the spatial pattern of imperviousness and rain are neglected. The various imperviousness scenarios we examined led to significant changes in the hydrographs at the two gaged locations after accounting for uncertainties in the parameters and initial condition. The changes consisted of delays in the time to peak at the overall outlet and increases in the peak flows at the internal gage location. Overall, the results indicate the spatial distribution of imperviousness can have an important effect on the hydrologic response, and point to the need for including both the spatial variability of rainfall and imperviousness when determining the hydrologic response of urbanizing basins.

ACKNOWLEDGEMENT

We gratefully acknowledge the U.S. Environmental Protection Agency's support of this project through grant number, RD83334601.

REFERENCES

- Ambrose B, Beven K, Freer J. 1996. Toward a generalization of the TOPMODEL concepts: topographic indices of hydrological similarity. *Water Resources Research* **32**(7): 2135–2145.
- Beven KJ, Binley A. 1992. The future of distributed models: model calibration and uncertainty prediction. *Hydrological Processes* **6**: 279–298.
- Beven KJ, Kirkby MJ. 1979. A physically based variable contributing area model of basin hydrology. *Hydrological Science Journal* **24**(1): 43–69.
- Brutsaert W, Nieber JL. 1977. Regionalized drought flow hydrographs from a mature glaciated plateau. *Water Resources Research* **13**: 637–643.
- Burges SJ, Wigmosta MS, Meena JM. 1998. Hydrological effects of land-use change in a zero-order catchment. *Journal of Hydrologic Engineering* **3**(2): 86–97. DOI: 10.1061/(ASCE)1084-0699(1998)3:2(86).
- Claggett PR, Jantz CA, Goetz SJ, Bisland C. 2004. Assessing development pressure in the Chesapeake Bay watershed: an evaluation of two land use change models. *Environmental Monitoring and Assessment* **94**: 129–146.
- Cuo L, Lettenmaier DP, Mattheussen BV, Storck P, Wiley M. 2008. Hydrologic prediction for urban watersheds with the distributed hydrology-soil—vegetation model. *Hydrological Processes* **22**(21): 4205–4213.
- DeFries R, Eshleman KN. 2004. Land-use change and hydrologic processes: a major focus for the future. *Hydrological Processes* **18**: 2183–2186.
- Delleur JW. 2003. The evolution of urban hydrology: past, present, and future. *Journal of Hydraulic Engineering* **129**(8): 563–573. DOI: 10.1061/(ASCE)0733-9429(2003)129:8(563).
- Dingman SL. 1994. *Physical Hydrology*. Macmillan: New York.
- D'Odorico P, Rigon R. 2003. Hillslope and channel contributions to the hydrologic response. *Water Resources Research* **39**(5): 1113. DOI:10.1029/2002WR001708.
- Duan J, Miller N. 1997. A generalized power function for the subsurface transmissivity profile in TOPMODEL. *Water Resources Research* **33**(11): 2559–2562.
- Easton ZM, Gérard-Marchant P, Walter MT, Petrovic AM, Steenhuis TS. 2007. Hydrologic assessment of an urban variable source watershed in the northeast United States. *Water Resources Research* **43**: W03413. DOI: 10.1029/2006WR005076.
- Ewen J, Parkin G. 1996. Validation of catchment models for predicting land-use and climate change impacts. 1. Method. *Journal of Hydrology* **175**(1–4): 583–594.
- Franchini M, Wendling J, Oblad C, Todini E. 1996. Physical interpretation and sensitivity analysis of the TOPMODEL. *Journal of Hydrology* **175**(1–4): 293–338.
- Guo Y, Adams B. 1998. Hydrologic analysis of urban catchments with event-based probabilistic models 1. Runoff volume. *Water Resources Research* **34**(12): 3421–3431.
- Homer R, Dewitz J, Fry J, Coan M, Hossain N, Larson C, Herold N, McKerron A, VanDriel JN, Wickham J. 2007. Completion of the 2001 National Land Cover Database for the conterminous United States. *Photogrammetric Engineering and Remote Sensing* **73**(4): 337–341.
- Leopold LB. 1968. *Hydrology for Urban Land Planning—A Guidebook on the Hydrologic Effects of Urban Land Use*. U.S. Geological Survey Circular 554. USGS: Reston, Virginia.
- Leopold LB, Maddock T. 1953. *The Hydraulic Geometry of Stream Channels and Some Physiographic Implications*. U.S. Geological Survey Professional Paper 252. USGS: Washington, DC.
- McCuen R, Snyder W. 1975. A proposed index for comparing hydrographs. *Water Resources Research* **11**(6): 1021–1024.
- Mejia AI, Moglen GE. 2009. Spatial patterns of urban development from optimization of flood peaks and imperviousness-based measures. *Journal of Hydrologic Engineering* **14**(4): 416–424.
- Mikkelsen PS, Madsen H, Arnbjerg-Nielsen K, Rosbjerg D, Harrmøes P. 2005. Selection of regional historical rainfall time series as input to urban drainage simulation at ungauged locations. *Atmospheric Research* **77**(1–4): 4–17.
- Miller CV, Gutiérrez-Magness AL, Feit Majedi BL, Foster GD. 2007. *Water Quality in the Upper Anacostia River, Maryland: Continuous and Discrete Monitoring with Simulations to Estimate Concentrations and Yields, 2003-05*. U.S. Geological Survey Scientific Investigation Report 2007–5142. USGS: Reston, Virginia.
- Milly P. 1986. An event-based simulation model of moisture and energy fluxes at a bare soil surface. *Water Resources Research* **22**(12): 1680–1692.

- Moglen GE, Beighley RE. 2002. Spatially explicit hydrologic modeling of land use change. *Journal of the American Water Resources Association* **38**(1): 241–253.
- Moglen GE, Shivers DE. 2006. *Methods for Adjusting U.S. Geological Survey Rural Regression Peak Discharges in an Urban Setting*. U.S. Geological Survey Scientific Investigations Report 2006–5270. USGS: Reston, Virginia.
- Moglen GE, Thomas WO, Cuneo CG. 2006. *Evaluation of Alternative Statistical Methods for Estimating Frequency of Peak Flows in Maryland*. Maryland Department of Transportation Final Report (SP907C4B). MDSA: Baltimore, Maryland.
- Montgomery DR, Dietrich WE. 1988. Where do channels begin? *Nature* **336**: 232–234.
- Nash JE, Sutcliffe JV. 1970. River flow forecasting through conceptual models part I—a discussion of principles. *Journal of Hydrology* **10**(3): 282–290. DOI: 10.1016/0022-1694(70)90255-6.
- National Oceanic and Atmospheric Administration. 2008a. *MARFC Operational NEXRAD Stage-III Data*. http://dipper.nws.noaa.gov/hdsb/data/nexrad/marfc_stageiii.php. Accessed October 2008.
- National Oceanic and Atmospheric Administration. 2008b. *NCDC Storm Event Database*. <http://www4.ncdc.noaa.gov/cgi-win/wwcgi.dll?wwEvent~Storms>. Accessed October 2008.
- National Oceanic and Atmospheric Administration. 2008c. *Point Precipitation Frequency Estimates from NOAA Atlas 14 for Maryland*. <http://www.nws.noaa.gov/oh/hdsc/index.html>. Accessed October 2008.
- Natural Resources Conservation Service. 2008a. *Soil Survey Geographic Database (SSURGO)*. <http://soils.usda.gov/survey/geography/ssurgo/>. Accessed September 2008.
- Natural Resources Conservation Service. 2008b. *State Soil Geographic (STATSGO) Database for Maryland*. <http://soildatamart.nrcs.usda.gov>. Accessed September 2008.
- Nicótiña L, Alessi Celegon E, Rinaldo A, Marani M. 2008. On the impact of rainfall patterns on the hydrologic response. *Water Resources Research* **44**: W12401. DOI: 10.1029/2007WR006654.
- Olivera F, Maidment D. 1999. Geographic Information Systems (GIS)-based spatially distributed model for runoff routing. *Water Resources Research* **35**(4): 1155–1164.
- Philip JR. 1960. The theory of infiltration. In *Advances in Hydrosience*, Chow VT (ed). Academic Press: Orlando, Florida; 215–296.
- Pielke RA. 2005. Land use and climate change. *Science* **310**(5754): 1625–1626.
- Poff NL, Bledsoe BP, Cuhaciyan CO. 2006. Hydrologic variation with land use across the contiguous United States: geomorphic and ecological consequences for stream ecosystems. *Geomorphology* **79**: 264–285.
- Rinaldo A, Rodríguez-Iturbe I. 1996. Geomorphological theory of the hydrological response. *Hydrological Processes* **10**(6): 803–829.
- Rodríguez F, Cudennec C, Andrieu H. 2005. Application of morphological approaches to determine unit hydrographs of urban catchments. *Hydrological Processes* **19**(5): 1021–1035.
- Rodríguez-Iturbe I, Valdés JB. 1979. The geomorphologic structure of hydrologic response. *Water Resources Research* **15**: 1409–1420.
- Rossman LA. 2007. *Storm Water Management Model User's Manual Version 5-0*, EPA/600/R-05/040. United States Environmental Protection Agency: Cincinnati, OH.
- Saco PM, Kumar P. 2002. Kinematic dispersion in stream networks: 1. Coupling hydraulic and network geometry. *Water Resources Research* **38**(11): 1244. DOI: 10.1029/2001WR000695.
- Sauer VB, Thomas WO, Stricker VA, Wilson KV. 1983. *Flood Characteristics of Urban Watersheds in the United States*. U.S. Geological Survey Water Supply Paper 2207. USGS: Reston, Virginia.
- Segond ML, Wheeler HS, Onof C. 2007. The significance of spatial rainfall representation for flood runoff estimation: a numerical evaluation based on the Lee catchment, UK. *Journal of Hydrology* **347**(1–2): 116–131. DOI: 10.1016/j.jhydrol.2007.09.040.
- Smith JA, Baeck ML, Meierdiercks KL, Nelson PA, Miller AJ, Holland EJ. 2005. Field studies of the storm event hydrologic response in an urbanizing watershed. *Water Resources Research* **41**: W10413. DOI: 10.1029/2004WR003712.
- Stern JE. 1990. State plane coordinate system of 1983. *NOAA Manual NOS NGS 5*. U.S. Department of Commerce: Rockville, Maryland.
- Szilagyi J, Parlange MB. 1998. Baseflow separation based on analytical solutions of the Boussinesq equation. *Journal of Hydrology* **204**: 251–260.
- Tarboton D. 1997. A new method for the determination of flow directions and upslope areas in grid digital elevation models. *Water Resources Research* **33**(2): 309–319.
- Tenenbaum DE, Band LE, Kenworthy ST, Tague CL. 2006. Analysis of soil moisture patterns in forested and suburban catchments in Baltimore, Maryland, using high-resolution photogrammetric and LIDAR digital elevation datasets. *Hydrological Processes* **20**(2): 219–240.
- Toprak ZF, Cigizoglu HK. 2008. Predicting longitudinal dispersion coefficient in natural streams by artificial intelligence methods. *Hydrological Processes* **22**(20): 4106–4129.
- Troch PA, Smith JA, Wood EF, de Troch FP. 1994. Hydrologic controls of large floods in a small basin. *Journal of Hydrology* **156**: 285–309.
- U.S. Environmental Protection Agency and U.S. Geological Survey. 2006. *National Hydrography Dataset Plus*. <http://www.horizonsystems.com/nhdplus/index.php>. Accessed October 2008.
- U.S. Geological Survey. 2008a. *Instantaneous Data Archive (IDA)*. <http://ida.water.usgs.gov/ida/>. Accessed September 2008.
- U.S. Geological Survey. 2008b. National Elevation Dataset, <http://gisdata.usgs.net/ned>. Accessed September 2008.
- U.S. Geological Survey. 2008c. National Land Cover Database 2001, <http://www.mrlc.gov/index.asp>. Accessed September 2008.
- Valeo C, Moin S. 2001. Hortonian and variable source area modeling in urbanizing basins. *Journal of Hydrologic Engineering* **6**(4): 328335. DOI: 10.1061/(ASCE)1084-0699(2001)6:4(328).
- Vörösmarty CJ, Green P, Salisbury J, Lammers RB. 2000. Global water resources: vulnerability from climate change and population growth. *Science* **289**(5477): 284–288. DOI: 10.1126/science.289.5477.284.
- Vrugt JA, Gupta HV, Bouten W, Sorooshian S. 2003. A shuffled complex evolution metropolis algorithm for optimization and uncertainty assessment of hydrologic model parameters. *Water Resources Research* **39**(8): 1201. DOI: 10.1029/2002WR001642.
- Wagner T, Wheeler HS, Lees MJ. 2004. *Monte-Carlo Analysis Toolbox User Manual*. Penn State University, formerly Imperial College: University Park, PA.
- Walsh CJ, Roy AH, Feminella JW, Cottingham PD, Groffman PM, Morgan RP II. 2005. The urban stream syndrome: current knowledge and the search for a cure. *Journal of the North American Benthological Society* **24**(3): 706–723.
- Woods R, Sivapalan M. 1999. A synthesis of space-time variability in storm response: rainfall, runoff generation, and routing. *Water Resources Research* **35**(8): 2469–2485.